Photodissolution of ferrihydrite in the presence of oxalic acid: An in situ ATR−FTIR/DFT study

ARTICLE *in* LANGMUIR · NOVEMBER 2010

Impact Factor: 4.46 · DOI: 10.1021/la101357y · Source: PubMed

4 AUTHORS, INCLUDING:

Narayan Bhandari
Rice University
14 PUBLICATIONS **134** CITATIONS
SEE PROFILE

J. D. Kubicki
University of Texas at El Paso
217 PUBLICATIONS **4,452** CITATIONS
SEE PROFILE

Langmuir
Article
pubs.acs.org/Langmuir

Photodissolution of Ferrihydrite in the Presence of Oxalic Acid: An In Situ ATR-FTIR/DFT Study†

Narayan Bhandari,[‡] Douglas B. Hausner,[‡,§] James D. Kubicki,[∥] and Daniel R. Strongin*[,‡]

[‡]*Department of Chemistry, Temple University, Philadelphia, Pennsylvania 19122,* [§]*Department of Chemistry, Rutgers Camden, 315 Penn Street, Camden, New Jersey 08102, and* [∥]*Department of Geosciences, The Pennsylvania State University, University Park, Pennsylvania 16802*

Received April 6, 2010. Revised Manuscript Received June 11, 2010

The photodissolution of the iron oxyhydroxide, ferrihydrite, in the presence of oxalic acid was investigated with vibrational spectroscopy, density functional theory (DFT) calculations, and batch geochemical techniques that determined the composition of the solution phase during the dissolution process. Specifically, in situ attenuated total reflection Fourier transform infrared spectroscopy (ATR- FTIR) was used to determine the structure of the adsorbed layer during the dissolution process at a solution pH of 4.5. DFT based computations were used to interpret the vibrational data associated with the surface monolayer in order to help determine the structure of the adsorbed complexes. Results showed that at pH 4.5, oxalate adsorbed on ferrihydrite adopted a mononuclear bidentate (MNBD) binding geometry. Photodissolution at pH 4.5 exhibited an induction period where the rate of Fe(II) release was limited by a low concentration of adsorbed oxalate due to the site-blocking of carbonate that was intrinsic to the surface of the ferrihydrite starting material. Oxalate displaced this initial carbonate over time, and the dissolution rate showed a corresponding increase. Irradiation of oxalate/ferrihydrite at pH 4.5 also ultimately led to the appearance of carbonate reaction product (distinct from carbonate intrinsic to the starting material) on the surface.

1. Introduction

The dissolution of ferric iron bearing oxide/oxyhydroxide phases in aqueous systems plays an important role in the formation of bioavailable iron.[1] Reductive dissolution of ferric iron bearing oxide phases is particularly important because it results in the liberation of soluble ferrous iron. In general, the reductive dissolution of Fe(III) (hydr)oxides in the presence of organic ligands is an order of magnitude faster than nonreductive dissolution mechanisms (e.g., proton-promoted or ligand-promoted thermal dissolution).[1] The conversion of ferric iron into labile and bioavailable ferrous iron can be considerably enhanced in many chemical environments by photoreductive mechanisms.[2,3] Day, night, and seasonal variations in the concentration of ferrous and ferric iron in aquatic environments emphasize the role of light (in this case solar radiation) in the reductive dissolution of iron (oxy)hydroxides.[4−6]

Organic carboxylic acids, such as oxalic acid [$(COOH)_2$ a focus of this contribution], facilitate the dissolution of iron (oxy)-hydroxides upon adsorption and subsequent exposure to light. Based on prior research that has generally relied on inferences from kinetic measurements, Sulzberger and co-workers have proposed two possible mechanisms for the photoreductive dissolution of iron (oxy)hydroxides in the presence of organic ligands such as oxalate (i.e., $C_2O_4^{2-}$).[1,7] In the first, oxalate derived surface complexes absorb light resulting in an electronically excited state that is followed by charge transfer resulting in the reduction of Fe(III) and the oxidation of oxalate. In a second scenario, bulk iron acts as a chromophore and takes part in the heterogeneous photoredox reaction. It has been proposed that either mechanistic case results in the formation of reduced iron, CO_2, and the radical species $CO_2^{\bullet-}$.[1] Prior studies of iron oxy/hydroxide phases also have suggested that light absorption can lead to the formation of photoelectrons that are able to reduce Fe(III).[8,9] This process is believed to be limited by the recombination of the photoelectron in the conduction band with a valence band hole.[9]

Mineral phases interact with a wide range of aqueous phase species in natural environments. The presence and or prevalence of these species can potentially vary significantly, though some such as CO_2/CO_3^{2-} will be found in nearly all systems exposed to solar radiation. The adsorption of species, such as carbonate, on mineral surfaces may facilitate or inhibit dissolution processes.[10] Recently, it has been shown that nanoscale iron (oxy)hydroxide minerals exhibit particularly high reactivity toward CO_2 gas in forming surface adsorbed carbonate species,[11−13] indicating that minerals synthesized under ambient conditions in the laboratory may have significant amounts of adsorbed carbonate occupying reactive surface sites. If the extent of surface occupation by such

† Part of the Molecular Surface Chemistry and Its Applications special issue.

*To whom correspondence should be addressed. E-mail: dstrongi@temple.edu.

(1) Siffert, C.; Sulzberger, B. *Langmuir* **1991**, *7*(8), 1627–1634.
(2) Waite, T. D.; Morel, F. M. M. *Environ. Sci. Technol.* **1984**, *18*(11), 860–868.
(3) Borer, P.; Sulzberger, B.; Hug, S. J.; Kraemer, S. M.; Kretzschmar, R. *Environ. Sci. Technol.* **2009**, *43*(6), 1864–1870.
(4) McKnight, D. M.; Kimball, B. A.; Bencala, K. E. *Science* **1988**, *240*(4852), 637–40.
(5) Sullivan, A. B.; Drever, J. I.; McKnight, D. M. *J. Geochem. Explor.* **1998**, *64* (1−3), 141–145.
(6) McKnight, D. M.; Bencala, K. E. *Arct. Alp. Res.* **1988**, *20*(4), 492–500.
(7) Sulzberger, B.; Laubscher, H. *Mar. Chem.* **1995**, *50*(1- 4), 103–115.
(8) Sherman, D. M. *Geochim. Cosmochim. Acta* **2005**, *69*(13), 3249–3255.
(9) Leland, J. K.; Bard, A. J. *J. Phys. Chem.* **1987**, *91*(19), 5076–5083.
(10) Ganor, J.; Lasaga, A. C. *Geochim. Cosmochim. Acta* **1998**, *62*(8), 1295–1306.
(11) Baltrusaitis, J.; Grassian, V. H. *J. Phys. Chem. B* **2005**, *109*(25), 12227–12230.
(12) Villalobos, M.; Leckie, J. O. *J. Colloid Interface Sci.* **2001**, *235*(1), 15–32.
(13) Hausner, D. B.; Bhandari, N.; Pierre-Louis, A.-M.; Kubicki, J. D.; Strongin, D. R. *J. Colloid Interface Sci.* **2009**, *337*(2), 492–500.

species is significant, then the ability of other reactive ligands to compete for surface adsorption sites becomes a relevant issue. In the present study, for example, a question that is answered is does carbonate, ubiquitous to the ferrihydrite surface, affect the photoinduced dissolution of the mineral in the presence of an environmentally relevant reductant such as oxalate?

Numerous studies within the literature using in situ IR demonstrate its ability to elucidate molecular level processes occurring on mineral surfaces.[14−20] To the best of our knowledge, this contribution presents the first in situ IR study of the photodissolution of ferrihydrite nanoparticles in the presence of oxalate. We present research that investigates the surface chemistry of oxalate on the iron oxyhydroxide ferrihydrite, with attenuated total reflection Fourier transform infrared spectroscopy (ATR-FTIR), density functional theory (DFT) calculations, and batch geochemical reaction measurements. Ferrihydrite is a naturally occurring nanoscale iron oxyhydroxide mineral which typically ranges from 2 to 6 nm in diameter and is commonly found in both natural and industrial systems.[21] The in situ ATR-FTIR results coupled with DFT calculations allow us to infer the structure of adsorbed oxalate on ferrihydrite and the resulting reaction product upon irradiation. Prior studies have shown that ferrihydrite synthesized in carbonate containing solution or exposed to the ambient atmosphere results in a layer of carbonate.[11−13] Hence, we focus on the interaction of adsorbed carbonate/ferrihydrite with oxalate in this study, because of its presumed environmental relevance. We, however, contrast the reactions on this surface with ferrihydrite without an initial carbonate layer to discern the effects of the intrinsic carbonate layer on ferrihydrite. Overall, we feel that the results from this contribution add to our understanding of the photoinduced dissolution of iron oxyhydroxides in the presence of oxalate. Our results will show that the presence of adsorbed carbonate affects the photodissolution of ferrihydrite at a pH near 4 in the presence of light.

2. Experimental Section

Ferrihydrite used in this study was of the 2-line variety, a label that loosely refers to the number of broad Bragg peaks associated with its diffraction pattern. The ∼2 nm particles were prepared in two forms (normal and CO_2/carbonate-free) using a modified version of the method developed by Cornell and Schwartzman.[22] Throughout this contribution, we refer to these two forms as normal ferrihydrite and carbonate-free ferrihydrite. In either synthesis, 1 M NaOH was added to 0.1 M solution of $FeCl_3$ with constant stirring until the pH reached 7.5, which resulted in a blood-red suspension. The suspension was dialyzed with deionized water (18 MΩ cm^{-1}) for 4−5 days to remove counterions, centrifuged, and then air-dried. Carbonate-free ferrihydrite was prepared following the same method, but CO_2-free water was used and the ferrihydrite was never exposed to the ambient atmosphere (any transfer or reaction was performed in a N_2 environment). Vibrational spectra of these two types of ferrihydrite will be shown later. Brunauer−Emmett−Teller (BET) surface area measurements of ferrihydrite synthesized in our laboratory yielded average values of 320 ± 20 m^2/g, consistent with reported literature values.[22] Transmission electron microscopy (TEM) and X-ray diffraction (XRD) data confirmed that the size and crystallinity of the synthesized ferrihydrite was consistent with what was expected for 2-line ferrihydrite.[23] All chemicals used, sodium chloride, sodium oxalate, ferric chloride, sodium carbonate, sodium hydroxide, and hydrochloric acid, were obtained from Sigma Aldrich (analytical grade) and were used without additional purification. All solutions unless otherwise stated contained 5 mM NaCl.

Batch photodissolution experiments were performed in a Pyrex vessel (400 mL) using 200 mg of ferrihydrite in a total volume of 250 mL. The solution pH was maintained at 4.5 with a pH stat (718 STAT Titrino, Metrohm, Switzerland) using 1 M HCl as the titrant. A positive pressure of N_2 gas was maintained to ensure anoxic reaction conditions for 30 min prior to and during irradiation. The radiation source used was a 900 W high-pressure xenon lamp (Schoeffel Instruments, Westwood, NJ). A 4.5 m long fiber optic (Fiber Bundle Focusing Assemblies, Newport) was used to guide the light to the solution of interest. The incident radiation coming out of the fiber optic was analyzed using a BRC111A high speed CCD spectrometer (B & W TEK, Inc.), and a maximum light output was observed at a wavelength of 500 nm. Using a Melles Griot (USA) 30 W broadband power meter, the power density impinging on the reaction solution was measured to be 1.4 W/m^2. Pyrex glass was used as a cut-off filter for UV light,[3] and a water jacket was placed between the fiber optic and solution of interest to maintain a constant temperature (25 ± 1 °C). Collected samples were centrifuged and filtered through a Millipore filter (0.2 μm) and analyzed by spectrophotometric methods[24,25] for the determination of dissolved Fe(II).

ATR-FTIR spectra were collected using a Smart Orbit ATR (Thermo Scientific) diamond accessory and a Nicolet 6700 spectrometer (Thermo Scientific) equipped with a DTGS detector. In situ ATR-FTIR photodissolution experiments were carried out by first drying a film of ferrihydrite (∼1 mg) on a diamond ATR element in a N_2 environment. A Teflon flow cell (volume capacity ∼2 mL) that surrounded the dry film allowed the passage (at a rate of 30 mL/h) of solution. In all the FTIR experiments, data were collected as a single beam (resolution 4 cm^{-1}) of 80 co-added scans.

Quantum chemical geometry optimization and vibrational frequency calculations of adsorbed oxalate on iron clusters were performed using DFT with the program Gaussian 03 E.01[26] at the B3LYP/6-31G**[27−30] (and references therein) level of theory. Model clusters, $Fe_2H_{12}O_8$, containing two octahedrally coordinated Fe atoms connected via two Fe−(OH)−Fe linkages were

(14) Axe, K.; Vejgarden, M.; Persson, P. *J. Colloid Interface Sci.* **2006**, *294*(1), 31–37.
(15) Axe, K.; Persson, P. *Geochim. Cosmochim. Acta* **2001**, *65*(24), 4481–4492.
(16) Borer, P.; Hug, S. J.; Sulzberger, B.; Kraemer, S. M.; Kretzschmar, R. *Geochim. Cosmochim. Acta* **2009**, *73*(16), 4661–4672.
(17) Degenhardt, J.; McQuillan, A. J. *Chem. Phys. Lett.* **1999**, *311*(3,4), 179–184.
(18) Yoon, T. H.; Johnson, S. B.; Musgrave, C. B.; Brown, G. E. *Geochim. Cosmochim. Acta* **2004**, *68*(22), 4505–4518.
(19) Borda, M. J.; Strongin, D. R.; Schoonen, M. A. *Spectrochim. Acta, Part A* **2003**, *59A*(5), 1103–1106.
(20) Hug, S. J.; Sulzberger, B. *Langmuir* **1994**, *10*(10), 3587–3597.
(21) Jambor, J. L.; Dutrizac, J. E. *Chem. Rev.* **1998**, *98*(7), 2549–2585.
(22) Cornell, R. M., Schwertmann, U. *The Iron Oxides: Structure, Properties, Reactions, Occurerences and Uses*, 2nd ed.; Wiley-VCH: Weinheim, 2003.
(23) Michel, F. M.; Ehm, L.; Antao, S. M.; Lee, P. L.; Chupas, P. J.; Liu, G.; Strongin, D. R.; Schoonen, M. A. A.; Phillips, B. L.; Parise, J. B. *Science* **2007**, *316* (5832), 1726–1729.
(24) Stookey, L. L. *Anal. Chem.* **1970**, *42*(7), 779–781.
(25) Hao, J.; Murphy, R.; Lim, E.; Schoonen, M. A. A.; Strongin, D. R. *Geochim. Cosmochim. Acta* **2009**, *73*(14), 4111–4123.
(26) Frisch, M. J.; Trucks, G. W.; Schlegel, H. B.; Scuseria, G. E.; Robb, M. A.; Cheeseman, J. R.; Montgomery, J. A., Jr.; Vreven, T.; Kudin, K. N.; Burant, J. C.; Millam, J. M.; Iyengar, S. S.; Tomasi, J.; Barone, V.; Mennucci, B.; Cossi, M.; Scalmani, G.; Rega, N.; Petersson, G. A.; Nakatsuji, H.; Hada, M.; Ehara, M.; Toyota, K.; Fukuda, R.; Hasegawa, J.; Ishida, M.; Nakajima, T.; Honda, Y.; Kitao, O.; Nakai, H.; Klene, M.; Li, X.; Knox, J. E.; Hratchian,H. P.; Cross, J. B.; Bakken, V.; Adamo, C.; Jaramillo, J.; Gomperts, R.; Stratmann, R. E.; Yazyev, O.; Austin, A. J.; Cammi, R.; Pomelli, C.; Ochterski, J. W.; Ayala, P. Y.; Morokuma, K.; Voth, G. A.; Salvador, P.; Dannenberg, J. J.; Zakrzewski, V. G.; Dapprich, S.; Daniels, A. D.; Strain, M. C.; Farkas, O.; Malick, D. K.; Rabuck, A. D.; Raghavachari, K.; Foresman, J. B.; Ortiz, J. V.; Cui, Q.; Baboul, A. G.; Clifford, S.; Cioslowski, J.; Stefanov, B. B.; Liu, G.; Liashenko, A.; Piskorz, P.; Komaromi, I.; Martin, R. L.; Fox, D. J.; Keith, T.; Al-Laham, M. A.; Peng, C. Y.; Nanayakkara, A.; Challacombe, M.; Gill, P. M. W.; Johnson, B.; Chen, W.; Wong, M. W.; Gonzalez, C.; Pople, J. A. *Gaussian 03*, revision E.01; Gaussian, Inc.: Wallingford, CT, 2004.
(27) Becke, A. D. *J. Chem. Phys.* **1993**, *98*(7), 5648–5652.
(28) Becke, A. D. *J. Chem. Phys.* **1993**, *98*(2), 1372–1377.
(29) Lee, C.; Yang, W.; Parr, R. G. *Phys. Rev. B: Condens. Matter* **1988**, *37*(2), 785–789.
(30) Rassolov, V. A.; Ratner, M. A.; Pople, J. A.; Redfern, P. C.; Curtiss, L. A. *J. Comput. Chem.* **2001**, *22*(9), 976–984.

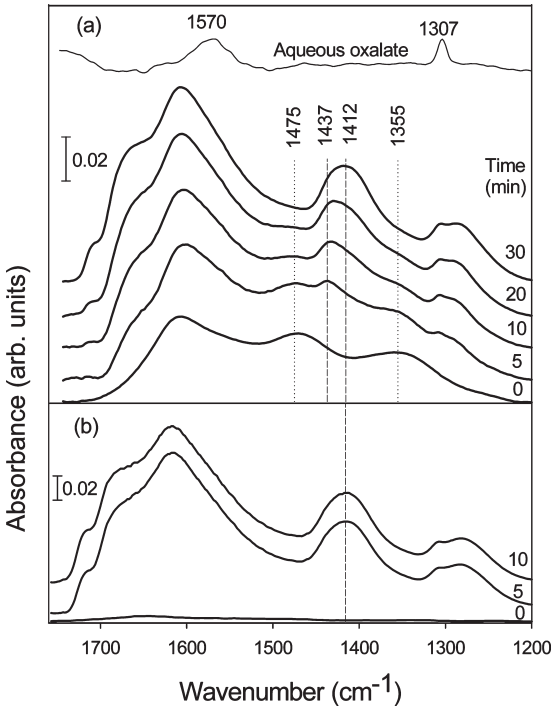

Figure 1. ATR-FTIR of aqueous oxalate and time dependent spectra of adsorbed oxalate on normal ferrihydrite (a) and time dependent spectra of adsorbed oxalate on carbonate-free ferrihydrite (b). The conditions were 5 mM oxalate, pH 4.5, 5 mM NaCl, and flow of 30 mL/h. The bottom spectrum (indicated as 0 min) in each case was ferrihydrite before exposure to oxalate. For the sake of clarity, the intensity (absorbance unit) of aqueous oxalate was multiplied by 4. Dashed lines near 1475 and 1355 cm^{-1} indicate the peak position of adsorbed carbonate species. The remaining two dotted lines indicate the shift in peak position of the $\nu_s(C-O) + \nu(C-C)$ oxalate combination mode during 30 min of flow. The spectra are offset for clarity.

used to represent the ferrihydrite particle surface. Previous studies in our laboratory[13,31,32] showed that calculated vibrational frequencies of different adsorbates (sulphite, carbonate, and ascorbate) on these Fe-hydroxide dimers correlate well with observed experimental IR frequencies of these adsorbates on ferrihydrite. Minima on the potential energy surfaces were located from potential energy minimization calculations on the entire system where no symmetry or geometrical constraints were allowed. To account for solvation effects, six H_2O molecules were incorporated in the cluster. Calculated frequencies were corrected by a scaling factor of 0.9613[18,33] and compared with experimentally observed vibrational frequencies.

3. Results and Discussion

3.1. ATR-FTIR of Oxalate in Solution and on Ferrihydrite in the Absence of Light. As a point of reference, the vibrational spectrum of an aqueous 5 mM sodium oxalate solution at pH 4.5 is shown in Figure 1a. Aqueous oxalate displays two strong vibrational modes at 1307 and 1570 cm^{-1} that are associated with the symmetric [$\nu_s(C-O)$] and asymmetric [$\nu_a(C-O)$] stretching modes, respectively.[14,15,18,20] Oxalic acid has a pK_{a1} and pK_{a2} of 0.97 and 3.57, respectively,[15] indicating that the deprotonated species, $C_2O_4^{2-}$, is the predominant solution phase species at pH 4.5 and above. The symmetry point group of the gaseous oxalate ion is D_{2h}, but upon solvation its symmetry has been suggested to be lowered to D_{2d}.[34,35] Figure 1a also shows the time dependent evolution of adsorbed oxalate modes as 5 mM oxalate was flowed over normal ferrihydrite, and Figure 1b shows the evolution of oxalate modes on carbonate-free ferrihydrite under the same experimental conditions. The bottom spectrum of Figure 1a is associated with ferrihydrite that has not yet been exposed to aqueous oxalate. Note that the modes associated with this spectrum near 1355 and 1475 cm^{-1} are associated with surface carbonate that adsorbs during the synthesis of the mineral or likewise occurs during the exposure of the iron oxyhydroxide to the ambient atmosphere.[13] These modes decrease upon exposure to oxalate, and after a 30 min exposure these bands are no longer apparent. In contrast, the modes attributable to adsorbed oxalate,[14] which are located near 1708 cm^{-1} [$\nu_s(C=O)$], 1668 cm^{-1} [$\nu_a(C=O)$], 1280 cm^{-1} [$\nu_a(C-O)$], and 1412 cm^{-1} [$\nu_s(C-O) + \nu(C-C)$ combination mode], increase in spectral intensity over the 30 min exposure time. In addition, vibrational modes at 1308 and 1610 cm^{-1}, which arise from hydrogen-bonded oxalate associated with the ferrihydrite surface, grow in over this same time frame. A closer inspection of the data also shows that the positions of the oxalate vibrational bands shift as the exposure time increases and the oxalate coverage increases. For example, the $\nu_s(C-O) + \nu(C-C)$ combination mode is located at 1437 cm^{-1} after a 5 min exposure to oxalate and its absorbance maximum shifts to 1412 cm^{-1} over a period of 30 min. The reason for this shift could be due to oxalate adsorbing on different binding sites on the ferrihydrite surface, a surface coverage effect, or lateral interactions between carbonate and oxalate that are ultimately eliminated due to the displacement of surface adsorbed carbonate. We favor the former possibility, since after the 30 min exposure the asymmetry of the $\nu_s(C-O) + \nu(C-C)$ mode does suggest that more than one type of adsorbed oxalate species contributes to the spectral intensity. We summarize our assignments in Table 1 in view of assignments made in prior research for oxalate on environmentally relevant metal oxide and metal (oxy)hydroxide mineral phases.

Figure 1b exhibits an ATR-FTIR spectrum of carbonate-free ferrihydrite (0 min spectrum) and of this surface after it was exposed to an oxalate flow for 5 and 10 min. Similar to oxalate adsorption on normal ferrihydrite, we associate the vibrational modes that appear at 1708 cm^{-1} [$\nu_s(C=O)$], 1668 cm^{-1} [$\nu_a(C=O)$], 1280 cm^{-1} [$\nu_a(C-O)$], and 1412 cm^{-1} [$\nu_s(C-O) + \nu(C-C)$ combination mode] to adsorbed oxalate. This specific data set shows, however, that oxalate adsorption on carbonate-free ferrihydrite is rapid compared to the adsorption process on normal ferrihydrite. Specifically, the oxalate modes grow to a maximum intensity after 5 min, while it takes at least 30 min to achieve a saturation coverage of oxalate on normal ferrihydrite under the same conditions. This direct comparison suggests that carbonate present on normal ferrihydrite slows the adsorption kinetics of oxalate compared to the same process on a carbonate-free surface.

3.2. DFT Vibrational Frequency Calculation and Identification of Adsorbed Complexes. To obtain a better understanding of the coordination geometry of the adsorbed oxalate complexes at the ferrihydrite/water interface, infrared vibrational frequencies were calculated. Specifically, vibrational frequencies were calculated for oxalate bound individually in three different possible inner-sphere binding geometries: (a) mononuclear monodentate (MNMD), (b) binuclear bidentate (BNBD) and (c)

(31) Liu, G.; Debnath, S.; Paul, K. W.; Han, W.; Hausner, D. B.; Hosein, H.-A.; Michel, F. M.; Parise, J. B.; Sparks, D. L.; Strongin, D. R. *Langmuir* **2006**, *22*(22), 9313–9321.
(32) Debnath, S.; Hausner, D. B.; Strongin, D. R.; Kubicki, J. *J. Colloid Interface Sci.* **2009**, *341*(2), 215–223.
(33) Wong, M. W. *Chem. Phys. Lett.* **1996**, *256*(4,5), 391–399.
(34) Hind, A. R.; Bhargava, S. K.; Van Bronswijk, W.; Grocott, S. C.; Eyer, S. L. *Appl. Spectrosc.* **1998**, *52*(5), 683–691.
(35) Begun, G. M.; Fletcher, W. H. *Spectrochim. Acta* **1963**, *19*(8), 1343–1439.

Table 1. Comparison of Inner-Sphere FTIR Peak Positions (cm^{-1}) for Adsorbed Oxalate on Various Metal Oxide/Oxyhydroxide Surfaces

adsorption system	ν_a(C−O)	ν_s(C−O) + ν(C−C)	ν_a(C=O)	ν_s(C=O)	ref
oxalate + chromium oxyhydroxide	1269	1405	1680	1708	17
oxalate + boehemite	1288	1413	1702	1722	15
oxalate + boehemite	1286	1418	1700	1720	18
oxalate + hematite	1305	1423	1701	1720	37
oxalate + lepidocrocite	1273	1407	1682	1710	36
oxalate + goethite	1255	1404	1692	1713	14
oxalate + ferrihydrite	1280	1412	1668	1708	this study

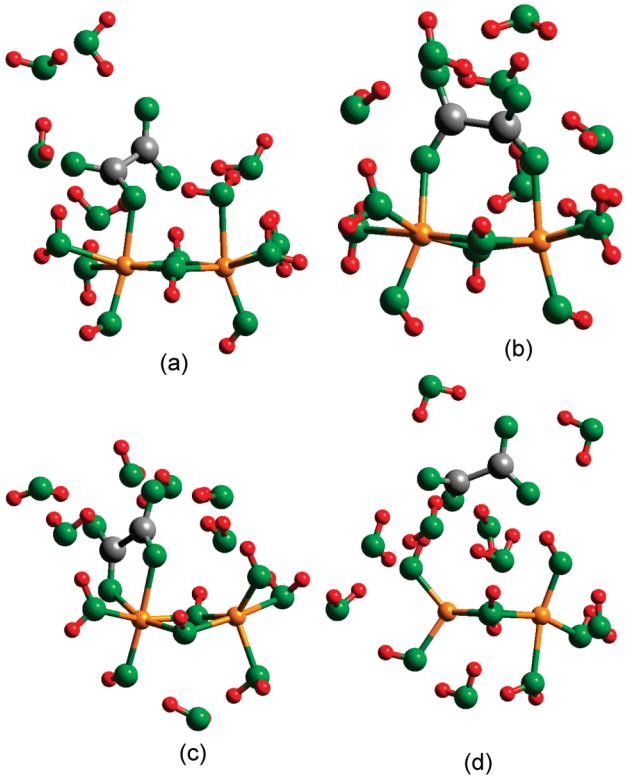

Figure 2. Optimized oxalate surface complex geometries on $Fe_2H_{24}O_{14}$ model clusters: (a) mononuclear monodentate (MNMD), (b) binuclear bidentate (BNBD), (c) mononuclear bidentate (MNBD), and (d) outer-sphere/hydrogen-bonded. Geometries were optimized at the B3LYP/6-31G** level using Gaussian 03. Graphics created with Cerius[2] (Accelrys Inc., San Diego, CA). Green atoms are oxygen, gray atoms are carbon, red atoms are hydrogen, and brown atoms are iron.

mononuclear bidentate (MNBD).[14,18,37] These adsorption geometries are depicted in Figure 2a−c. DFT calculations associated with these structures yield four distinct IR modes within the region of 1200−1800 cm^{-1}. Table 2 displays the calculated vibrational frequencies associated with these complexes and the experimentally observed IR frequencies within the region of 1200−1800 cm^{-1}. Figure 3 displays a plot of calculated versus experimental frequencies for the three different adsorption geometries. Among the three adsorption geometries, the plot suggests that the MNBD binding geometry (Figure 2c) has the best correlation with our experimentally determined frequencies based on an analysis of the slope, standard deviation, and R^2 correlation of the different plots (see Table 2). Among the three plots, the experimental frequency versus the calculated frequencies for the MNBD geometry plot is

Table 2. Comparisons of Observed Frequencies of Inner Sphere Oxalate at the Ferrihydrite/Water Interface and Calculated Frequencies (cm^{-1}) for the Geometry-Optimized Oxalate−$Fe_2H_{24}O_{14}$ Model Clusters[a]

modes	observed frequencies (cm^{-1})	calculated frequencies (cm^{-1}) BNBD	MNMD	MNBD
ν_a(C−O)	1280	1305 (25)	1239 (−41)	1280 (0)
ν_s(C−O) + ν(C−C)	1412	1443 (31)	1383 (−29)	1399 (−13)
ν_a(C=O)	1668	1570 (−98)	1597 (−71)	1674 (6)
ν_s(C=O)	1708	1683 (−25)	1680 (−28)	1687 (−21)
R^2	NA	0.984	0.947	0.996
slope	NA	0.806	0.772	0.986
intercept	NA	273.62	328.12	13.87
standard deviation	NA	54.34	62.75	14.67

[a] Differences between calculated and observed frequencies are given in parentheses.

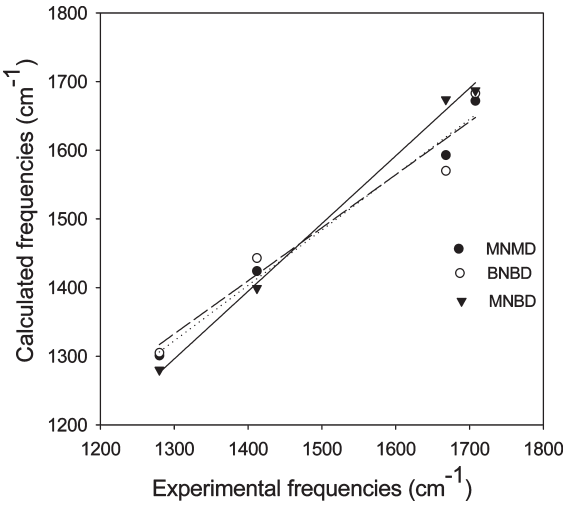

Figure 3. Linear regression plots that compare experimentally determined to calculated vibrational frequencies for the different geometries in Figure 2. Linear fit parameters are given in Table 2. On the basis of this analysis, the most probable coordination geometry of adsorbed oxalate on the ferrihydrite surface is MNBD.

associated with the lowest standard deviation (14.67), Y-intercept closest to zero (13.87, ideal value is zero), and best R^2 correlation (0.996). We infer from this analysis that adsorbed oxalate likely adopts a MNBD binding configuration on the ferrihydrite surface. These ATR-FTIR results, interpreted in view of DFT calculations, are in agreement with prior experimental studies that proposed a similar binding geometry for oxalate on other metal oxide/hydroxide mineral phases.[14,18,37]

While the calculated frequencies for the (MNBD) inner-sphere complex explain the four strong experimentally determined modes at 1280, 1412, 1668, and 1708 cm^{-1}, two other modes at 1308 and 1610 cm^{-1} are not accounted for by this binding geometry.

(36) Hug, S. J.; Bahnemann, D. *J. Electron Spectrosc. Relat. Phenom.* **2006**, *150* (2−3), 208–219.
(37) Duckworth, O. W.; Martin, S. T. *Geochim. Cosmochim. Acta* **2001**, *65*(23), 4289–4301.

Table 3. Comparisons of Observed Frequencies of Aqueous Phase and Outer-Sphere Oxalate at the Ferrihydrite/Water Interface and Calculated Frequencies (cm^{-1}) for the Geometry-Optimized Oxalate−$Fe_2H_{26}O_{16}$ Model Clusters[a]

modes	aqueous phase		outer-sphere	
	observed frequencies (cm^{-1})	calculated frequencies (cm^{-1})	observed frequencies (cm^{-1})	calculated frequencies (cm^{-1})
ν_s(C−O)	1307	1289 (−18)	1308	1287 (−21)
ν_a(C−O)	1570	1572 (3)	1610	1591 (−19)
$\Delta\nu$	263	283	302	304

[a] Differences between calculated and observed frequencies are given in parentheses.

Axe et al. who investigated the oxalate−goethite system assigned two peaks at similar positions (1582 and 1308 cm^{-1}) to H-bonded (or outer-sphere) oxalate interacting with the surface hydroxyl groups of goethite.[14] This assignment was based on the differences observed in experimentally determined IR spectra for the adsorbed layer that was collected at low and high pH. Our DFT calculations associated with a H-bonded oxalate species on a Fe−O cluster support this assignment. A schematic of the binding geometry used for this specific calculation is shown in Figure 2d. We also infer from calculation and experiment that an outer-sphere or H-bonded oxalate contributes to the oxalate/ferrihydrite vibrational spectrum. Specifically, the wavenumber difference between the calculated ν_a(C−O) and ν_s(C−O) mode for H-bonded oxalate is 304 cm^{-1} (see Table 3), close to the experimental difference of 302 cm^{-1} between the 1610 and 1308 cm^{-1} modes that contribute to the vibrational spectrum of oxalate on ferrihydrite. We point out that the oxalate adsorption results presented above do suggest that there may be more than one type of oxalate species bound on the ferrihydrite surface. For comparison to the DFT calculations, we have chosen the mode positions that dominate the vibrational spectrum obtained at saturation coverage (see Figure 1a).

3.3. In Situ ATR-FTIR of Oxalate on Ferrihydrite in the Presence of Light. *3.3.1. Irradiation of Oxalate/Ferrihydrite under Static Conditions*. In situ experiments were carried out that investigated the surface chemistry of oxalate on ferrihydrite during irradiation. Experimental data shown in Figure 4 are time dependent spectra associated with adsorbed oxalate on ferrihydrite. The data were obtained after a 5 mM oxalate solution was flowed for 5 min (30 mL/h) over the iron oxyhydroxide, after which time the flow was stopped and the irradiation process was started.

The bottom spectrum (0 min) was obtained in the absence of light and shows intense modes at 1285, 1429, 1610, 1668, and 1709 cm^{-1} as well as small contributions at 1475 and 1355 cm^{-1}, with the latter modes being attributed to surface carbonate. After 15 min of light exposure, the intensity of all the modes assigned to adsorbed oxalate increased significantly and modes located at 1475/1355 cm^{-1} decreased slightly (but not completely). Furthermore, the mode originally at 1430 cm^{-1} shifted to 1420 cm^{-1} during the first ~15 min of irradiation. With increasing exposure time to light, the position modes near 1285, 1610, 1668, and 1708 cm^{-1} started to decrease as modes attributable to adsorbed carbonate at 1475 and 1355 cm^{-1} showed an increase in intensity. In this study, no attempt was made to maintain a constant pH, and after 5 h of irradiation the final solution pH was measured to be ~7. This observation indicates that the carbonate formed after photolysis is a stable surface complex at pH ~ 7 which cannot be easily displaced by oxalate. While data are not shown, the flowing of 5 mM NaCl (pH 7) over the ferrihydrite after irradiation resulted in no significant loss of intensity for the 1475/1355 cm^{-1} peak pair, suggesting that these vibrational modes are associated with an inner-sphere carbonate complex.

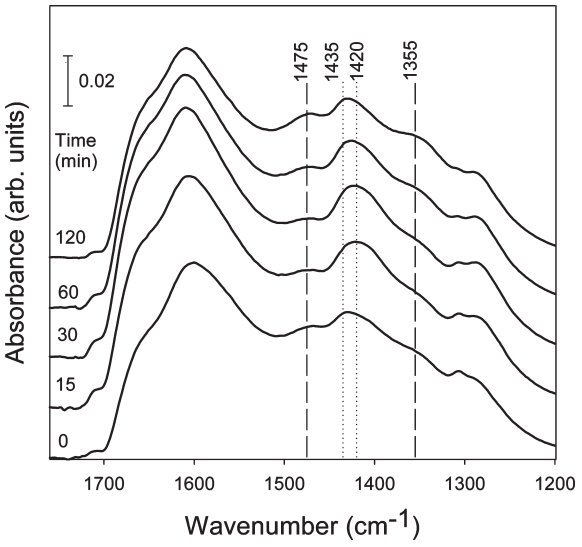

Figure 4. ATR-FTIR spectra recorded during the photodissolution of ferrihydrite in the presence of oxalate (5 mM) and light as a function of time. The experiment was carried out in static mode (nonflow conditions). The bottom spectrum was collected before irradiation of light (0 min), and subsequent spectra were collected at 15, 30, 60, and 120 min of light exposure. Vertical dashed lines indicate the peak positions associated with adsorbed carbonate species, and the dotted lines are associated with adsorbed oxalate [the ν_s(C−O) + ν(C−C) combination mode]. The spectra are offset for clarity.

3.3.2. Irradiation of Oxalate/Ferrihydrite under Flow Conditions. Figure 5 displays experimental results for photodissolution ATR-FTIR experiments where a 5 mM oxalate solution (5 mM NaCl at pH 4.5) was flowed over ferrihydrite in the dark until the system equilibrated (successive spectra showed no change), after which the sample was irradiated. Over the course of the irradiation, at least two experimental observations can be made. First, peaks attributable to surface carbonate increase during irradiation (at 1475 and 1355 cm^{-1}) during the 120 min exposure to radiation. Second, there is a continuous loss in intensity of the oxalate derived modes (noticeable near 1432 and 1285 cm^{-1}). We note that during these experiments a significant mass loss is believed to have occurred, based on an analysis of the loss of intensity of Fe−O stretching modes near 570 cm^{-1} (not shown). During control experiments (in dark), no shift and/or measurable intensity change indicative of mass loss occurred after attaining equilibrium.

3.3.3. Irradiation of an Oxalate Monolayer on Ferrihydrite. In addition to the above experiments where 5 mM of oxalate was maintained in the aqueous phase, experiments were carried out that investigated an adsorbed monolayer of oxalate (no solution phase oxalate) on the ferrihydrite surface at pH 4.5. For these experiments, normal ferrihydrite was exposed to a 5 mM oxalate solution at pH 4.5 for 30 min and then the oxalate

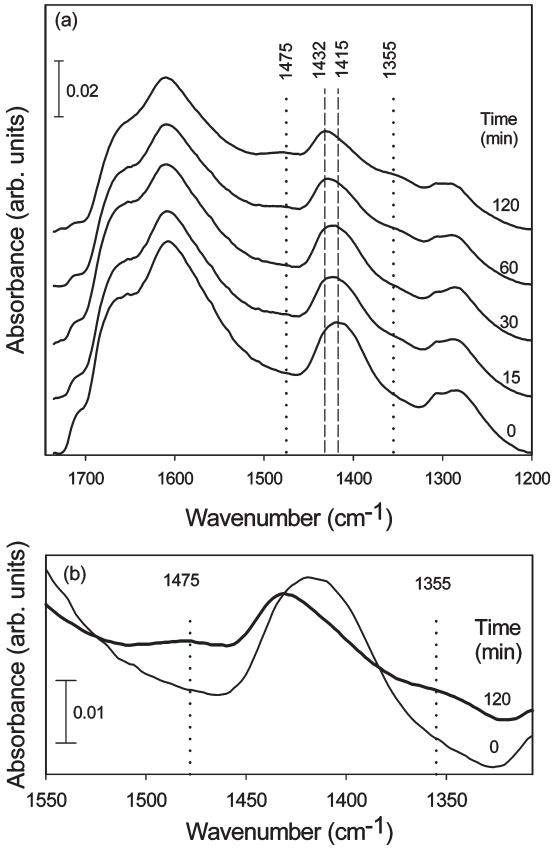

Figure 5. ATR-FTIR spectra recorded during the photodissolution of normal ferrihydrite at pH 4.5 in the presence of flowing oxalate as a function of time. Spectra were collected before irradiation (0 min) and after 15, 30, 60, and 120 min of light exposure (a). Dotted lines indicate the peak position of carbonate species adsorbed to ferrihydrite surface after photolysis, and the two dashed lines indicate the peak positions of modes associated with adsorbed oxalate. The spectra are offset for clarity. Also shown is an expanded region of the vibrational spectrum (b) to emphasize the growth of carbonate modes at 1475 and 1355 cm^{-1}, during irradiation.

solution was replaced by flowing pH 4.5 water. This particular type of experiment eliminated the possibility of oxalate adsorption from solution so that the behavior of the oxalate monolayer could be better isolated for study. Figure 6 shows that in the absence of solution phase oxalate modes assigned to oxalate decrease with time over the 180 min irradiation time. During the first 90 min of irradiation, the spectral peak maximum of the oxalate associated with the $\nu_s(C-O) + \nu(C-C)$ combination mode shifts from 1412 to 1430 cm^{-1}. This shift occurs alongside an increase in carbonate product that is associated with the 1475 and 1355 cm^{-1} features.[13,38] The contribution of the surface carbonate product to the vibrational spectra is greater than what was observed in the pH 4.5 flow experiments (Figure 5), since the displacement of surface oxalate by the adsorption of solution phase oxalate is not a possibility in these experiments. Oxalate decomposition is complete after 180 min of irradiation. Analysis of these specific data also addresses another issue concerning the composition and reactivity of the oxalate monolayer. Specifically, ATR-FTIR showed that oxalate may adopt two distinct binding sites on the ferrihydrite surface (see Figure 1a). These contributions are exhibited in the data as a spectral shoulder at 1430 cm^{-1} and a

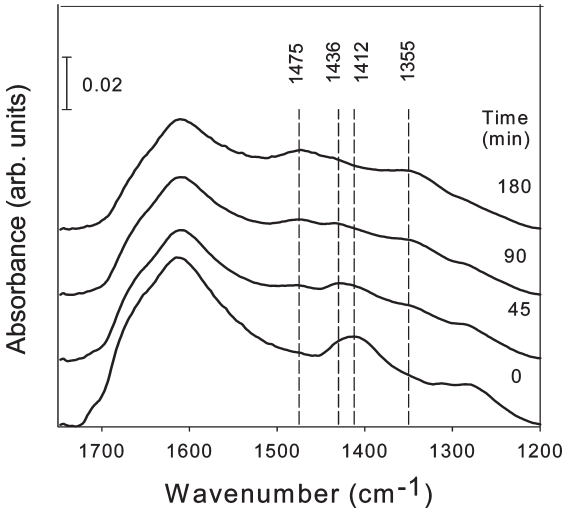

Figure 6. ATR-FTIR time dependent spectra showing the photolysis of an adsorbed oxalate monolayer on ferrihydrite in pH 4.5 water. Bottom spectrum (0 min) was collected before exposure to light, and subsequent spectra were collected at 45, 90, and 180 min of light exposure. The spectra are offset for clarity.

more prominent contribution at 1412 cm^{-1}. Based on data in Figure 1a, oxalate associated with the 1430 cm^{-1} mode is more significant at low coverage while oxalate exhibiting the mode at 1412 cm^{-1} dominates at the higher coverage. Data in Figure 6 demonstrate that the oxalate derived modes are completely eliminated after an irradiation time of 180 min, indicating that both oxalate species are photoactive and contribute to the photodissolution process. Discriminating between the binding details for the two proposed species will need to wait until a firm understanding of the ferrihydrite surface structure is developed through experiment and theory. Also of note is that the absorbance associated with the H-bonded (outer-sphere complex) species (characterized by the 1308 cm^{-1} mode) also decreases upon irradiation. This experimental observation suggests that either the H-bonded species converts to an inner-sphere complex or it desorbs from the mineral surface during irradiation.

3.4. Ferrihydrite Photodissolution/Photolysis Batch Study. Figure 7 shows results for the amount of Fe(II) release that occurs during batch dissolution experiments of ferrihydrite in the presence and absence of light with 5 mM oxalate in solution at pH 4.5 (anoxic conditions). As expected, the rate of light induced reductive dissolution was significantly higher than ligand-only promoted dissolution (no light), consistent with the results of previous investigations on other iron oxyhydroxides.[7,39] Control experiments (not presented in Figure 7) showed that ferrihydrite exhibited an insignificant amount of dissolution in the absence of oxalate, in the presence of light. Over the ~300 min of reaction time, our results based on three individual runs for each experimental condition show that the amount of aqueous Fe(II) that results from carbonate-free ferrihydrite is ~21 ± 1% more than that which results from normal ferrihydrite. We attribute this difference in amount of dissolution at least in part to the experimentally observed difference in the dissolution rates of the two surfaces within the first 30 min of reaction. As an estimate of the differences, a linear regression analysis of the dissolution data associated with normal ferrihydrite over a realtively short period of time (the first 30 min) leads to a calculated rate of $6.6 \pm 0.5 \times 10^{-5}$ mM/s. A similar analysis of the first 30 min of the data

(38) Bargar, J. R.; Kubicki, J. D.; Reitmeyer, R.; Davis, J. A. *Geochim. Cosmochim. Acta* **2005**, *69*(6), 1527–1542.

(39) Cwiertny, D. M.; Hunter, G. J.; Pettibone, J. M.; Scherer, M. M.; Grassian, V. H. *J. Phys. Chem. C* **2009**, *113*(6), 2175–2186.

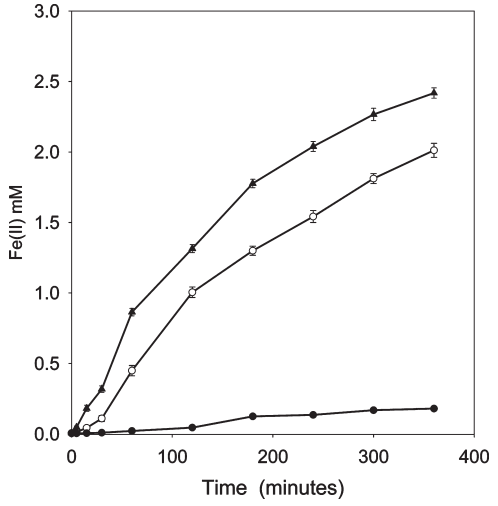

Figure 7. Dissolved Fe(II) production during the oxalate induced dissolution of carbonate-free ferrihydrite in the presence of light (filled triangles), normal ferrihydrite in the presence of light (open circles) and in the absence of light (filled circles) at pH 4.5. All experiments were carried out in an oxygen-free environment. In the case of carbonate-free ferrihydrite, Fe (II) release starts as soon as light exposure begins, but normal ferrihydrite exhibits an induction period where the amount of Fe(II) release is suppressed. For each plot, error bars represent one standard deviation from the average value of three individual experiments.

associated with carbonate-free ferrihydrite shows a dissolution rate during the first 30 min of $1.7 \pm 0.1 \times 10^{-4}$ mM/s, which is about 2.5 times greater than the dissolution rate associated with normal ferrihydrite. We believe that the lower amount of aqueous Fe(II) that results from the photodissolution of the normal ferrihydrite (relative to carbonate-free ferrihydrite) is due to the slower initial adsorption kinetics of oxalate due to the initial presence of carbonate. The ATR-FTIR results (Figure 1a) are consistent with this assertion, since they show that 30 min is required to attain a maximum coverage of oxalate on normal ferrihydrite, while no more than 5 min is required to achieve a maximum coverage if carbonate is not present (Figure 1b). There is an increase in the dissolution rate of normal ferrihydrite after this initial period, based on the experimental observation mentioned above that after 360 min of reaction there is only a 20% greater amount of Fe(II) resulting from the photodissolution of carbonate-free ferrihydrite than from normal ferrihydrite.

The photodissolution data shown in Figure 7 also show that the rate of photodissolution (proportional to the slope of the curve) shows a continuous decrease over the 360 min of reaction. This decrease is independent of the history of the ferrihydrite sample; that is, both normal and carbonate-free ferrihydrite show the same behavior. Over this 360 min of reaction, the mass of the ferrihydrite particle decreases by about 20%, which certainly plays a role in this decrease. We also suspect that the slow buildup of carbonate product on the surface of the ferrihydrite particles (see Figure 5) also contributes to the decrease. We surmise that the rate of carbonate production on the surface occurs at a faster rate than the displacement of this product by the adsorption of oxalate from solution. Unfortunately, distinguishing the relative contribution of mass loss due to dissolution and the blocking of surface sites by carbonate product is not possible from the data.

Figure 8 displays the amount of Fe(II) release as a function of time during the exposure of an oxalate monolayer on ferrihydrite at pH 4.5 to light (complementary to the ATR-IR derived data shown in Figure 6). The ferrihydrite sample that was used for this

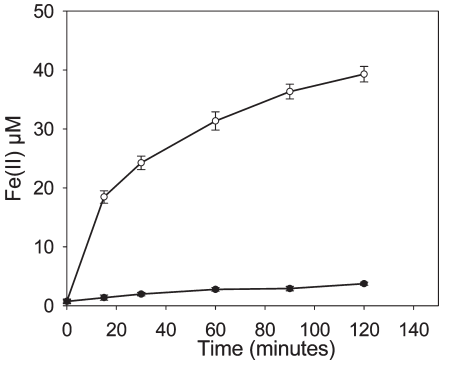

Figure 8. Time dependent Fe(II) release during the photolysis of an oxalate monolayer adsorbed on ferrihydrite surface (open circles) at a solution pH of 4.5. A control experiment (in the absence of light) also is shown (filled circles). For each plot, error bars represent one standard deviation from the average value of three individual experiments.

experiment was prepared in the same way as the ferrihydrite sample that was used to acquire the ATR-IR data in Figure 6. In short, ferrihydrite was exposed to oxalate for 30 min (which displaced surface carbonate), at which time the oxalate/ferrihydrite was resuspended in pH 4.5 water (no solution phase oxalate) and the system was irradiated. While the amount of Fe(II) release in the monolayer case is orders of magnitude less than that when oxalate is present in solution (see Figure 7), these data do show that the decrease in the surface oxalate concentration shown by ATR-FTIR in Figure 6 can be associated directly with the photoreduction of Fe(III) to Fe(II). We also feel these results are consistent with our contention made before when analyzing the data in Figure 6 that the entire oxalate monolayer, whether or not there are two distinct adsorbed oxalate species, contributes to the photoreduction process. We point out that, under the experimental conditions used in these experiments, there is no solution phase oxalate, so in contrast to data in Figure 7 the decreasing rate of photodissolution for this system after about 20 min can be attributed in large part to the decreasing concentration of oxalate during the irradiation process shown by the ATR-FTIR results in Figure 6. The amount of ferrihydrite mass loss in these experiments is estimated to be <1%, so the loss of surface area during the photodissolution is not expected to contribute to the loss in rate.

4. Summary and Implications

Oxalate induced photodissolution of ferrihydrite with adsorbed carbonate at pH 4.5 exhibited an induction period where the rate of Fe(II) release was limited by a low concentration of adsorbed oxalate due to the site-blocking of carbonate that was intrinsic to the surface of the starting material. Oxalate displaced this initial carbonate over time, and the dissolution rate showed a corresponding increase. In contrast, adsorption of oxalate as well as the initial photodissolution process on ferrihydrite that was prepared in a CO_2-free environment was faster relative to normal ferrihydrite. Irradiation of oxalate/ferrihydrite at pH 4.5 also ultimately led to the appearance of carbonate reaction product on the surface, and this surface bound product likely hinders the overall dissolution process at long reaction times by slowing down the adsorption of oxalate from solution.

The presence of a ubiquitous surface bound species such as carbonate may be relevant to prior studies that investigated the photodissolution of iron (oxy)hydroxides. Prior studies of the photodissolution of hematite,[1] hematite and goethite,[7] and

(nano- and microrods) goethite[39] in the presence of oxalate all showed an initial dissolution rate that was lower than the rate observed at longer reaction times. Sulzberger and Laubscher[7] proposed that the initial slower rate of dissolution that was followed by an increase in dissolution rate could be due to the autocatalytic effect of the Fe(II) photoproduct in thermal dissolution of the mineral. This thermal dissolution results in the formation of dissolved Fe(III)−oxalate complexes, which were postulated to be photoactive.[7] If this was the only reason for the slow initial kinetics that we experimentally observed for ferrihydrite, then the dissolution kinetics of normal and carbonate-free ferrihydrite should be similar. We, however, experimentally observe a higher photodissolution rate for carbonate-free ferrihydrite at early times. We speculate, based on our results, that the presence of species such as carbonate on the initial mineral surface may at least in part be a reason for the slower initial photodissolution kinetics that have been observed in earlier studies. In addition, iron oxides/oxyhydroxides are commonly used to remove toxic substances from the natural environments,[21] and we showed here that these nanomaterials prepared in the ambient atmosphere may contain an appreciable amount of surface carbonate. Carbonate is believed to be a well-known competitive inhibitor for the adsorption of many aqueous species, such as toxic species containing arsenic (As), lead (Pb), uranium (U), and so on.[40,41] In this context, it is suggested that special attention should be paid during the preparation of iron (oxy)hydroxide materials and use of contaminant-free (such as ubiquitous carbonate) nanomaterials may be highly efficient to remove the potentially dangerous species from natural environments.

In closing, we discuss our results further in the context of prior research that has proposed the following pathway for the reductive dissolution of the iron oxyhydroxide goethite. In the presence of light and oxalate under deaerated conditions,[7] it has been suggested that irradiation of a Fe(III)−oxalate surface complex leads to ligand-to-metal charge transfer, ultimately resulting in the reduction of structural Fe(III) to Fe(II) and the formation of CO_2 product. In the context of this reaction sequence, our experimental observations suggest that CO_2 product reacts to form carbonate surface complexes with surface Fe(III).

Whether carbonate product is bound on the same iron center(s) where oxalate was adsorbed initially cannot be determined from our results. However, it may be possible that iron atoms rather than those associated with initial oxalate binding might be released during photodissolution, via a shuttling of electrons through the bulk of the mineral. Recently, Yanima and Rosso showed that interfacial electron transfer reactions at one surface face can couple with another surface face via current flow through the crystal bulk especially in low band gap semiconductors such as iron oxy/hydroxides.[42] Reported values for the band gaps of 2-line ferrihydrite and hematite are ~2 eV,[31,42,43] suggesting that similar processes may be operative on a mineral such as ferrihydrite.

Acknowledgment. D.R.S. and J.D.K. greatly appreciate financial support from the National Science Foundation (NSF) Collaborative Research in Chemistry grant. In addition to NSF support (CHE0714121), D.R.S. appreciates partial support for this research from the Department of Energy, Basic Energy Sciences (DEFG029ER14644).

(40) Cheng, T.; Barnett, M. O.; Roden, E. E.; Zhuang, J. L. *Environ. Sci. Technol*. **2004**, *38*, 6059–6065.
(41) Appelo, C. A. J.; Van der Weiden, M. J. J.; Tournassat, C.; Charlet, L. *Environ. Sci. Technol*. **2002**, *36*(14), 3096–3103.
(42) Yanina, S. V.; Rosso, K. M. *Science* **2008**, *320*(5873), 218–222.
(43) Gilbert, B.; Frandsen, C.; Maxey, E. R.; Sherman, D. M. *Phys. Rev. B: Condens. Matter Mater. Phys*. **2009**, *79*(3), 035108-7.